# DiAna, an ImageJ tool for object-based 3D co-localization and distance analysis

Jean-François Gilles, Marc dos Santos, Thomas Boudier, Susanne Bolte, Nicolas Heck

HAL Id: hal-01408946

https://hal.sorbonne-universite.fr/hal-01408946

Submitted on 5 Dec 2016

**DiAna, an ImageJ tool for object-based 3D co-localization and distance analysis**

Jean-François Gilles[1], Marc Dos Santos[2], Thomas Boudier[3,4], Susanne Bolte[1,*], Nicolas Heck[2,*]

* Those authors equally contributed to his work

Affiliations

[1]Sorbonne Universités, UPMC University Paris 06, CNRS, Core Facility - Institut de Biologie Paris Seine (IBPS) 75005, Paris, France.

[2]Sorbonne Universités, UPMC Univ Paris 06, INSERM, CNRS, Neurosciences Paris Seine - Institut de Biologie Paris Seine (NPS - IBPS), 75005 Paris, France

[3]Sorbonne Universités, UPMC Univ Paris 06, IPAL, CNRS, Singapore.

[4]Bioinformatics Institute, Agency for science, technology and research (A*STAR), Singapore

Corresponding author

Nicolas Heck, Neuroscience Paris Seine, 7 quai Saint-Bernard, Building A 3rd floor, 75005 Paris, France.

Email: nicolas.heck@upmc.fr

**Abstract**

We present a new plugin for ImageJ called DiAna, for Distance Analysis, which comes with a user-friendly interface. DiAna proposes robust and accurate 3D segmentation for object extraction. The plugin performs automated object-based co-localization and distance analysis. DiAna offers an in-depth analysis of co-localization between objects and retrieves 3D measurements including co-localizing volumes and surfaces of contact. It also computes the distribution of distances between objects in 3D. With DiAna, we furthermore introduce an original method, which allows for estimating the statistical significance of object co-localization. DiAna offers a complete and intuitive 3D image analysis tool for biologists.

2

**1 Introduction**

Many biological and physiological studies depend on the analysis of the distribution and spatial relationship between biomarkers in a cell or tissue. Various methods, from immunodetection to transgene-driven expression of fluorescent proteins, allow to observe positive cells in whole specimen or tissue sections at the histological level, or to detect protein sub-cellular localization at the cellular level. The 3D-organization and relationship of these biomarkers can be investigated using fluorescence microscopy techniques that allow optical sectioning, such as confocal microscopy or multiphoton microscopy. These should be combined with appropriate image analysis methods. Biologists often investigate the spatial overlap of pairs of biomolecules in a cell or in a sub-cellular compartment by means of co-localization analysis, before inferring biological interaction and drawing functional conclusions.

Co-localization analysis can be carried out using two different, complementary methods: a pixel based approach [1][2] or an object-based approach [3][4][5], as well as a combination of the two approaches [6]. These methods have been reviewed in detail [5][7][8].

In the pixel-based approach, the linear relationship between a pair of biomolecules is calculated statistically between two fluorescent channels [2][9] without taking into account the positional information. Statistical significance of this correlation coefficient may be ensured by computing co-localization after scrambling pixel coordinates [10] or by shifting images pixel wise [11]. Pixel-based approaches are included in most commercially available image analysis softwares because they are easy to implement. However, co-localization analysis by pixel-based approaches is affected by the inherent noise of fluorescent images and thus not always applicable [5][8]. Furthermore, pixel-based approaches do not give information about the spatial relationship between objects.

In the object-based approach, spatial information is used to quantify the degree of co-localization between objects in the image. It is thus indispensable to perform segmentation prior to co-localization analysis in order to identify and delineate the objects of interest. Intensity thresholding is a simple method, but its easiness comes with limitations as the threshold is globally applied to the whole image. Recently, more sophisticated 3D, local segmentation methods have been developed [12][13], including spot segmentation and iterative thresholding, which we describe in this study.

The segmentation allows determining the volume that an object occupies in the 3D space as well as the localisation of the geometrical centroid or centre of mass of the object. The degree of co-localization can then be calculated in different ways, depending on the optical resolution limit and the size of objects investigated. In one approach co-localization is detected if the distance between the centres of the objects in two fluorescent channels is lower than image resolution. In another approach, co-localization can be inferred if the centre of one object falls into the volume occupied by the other object. These two paradigms are used in the JACOP plugin from ImageJ [5]. More recently, a plugin for object-based co-localization analysis has been implemented in the software Icy [8][14], In this approach, a spherical region is computed around the object centre, and co-localization is deduced if the centre of another object falls into this spherical region. Several drawbacks are inherent to the aforementioned approaches. Indeed, the object position determined by its centroid or centre of mass is not sufficient to fully represent the object. Furthermore, no information, neither on the extent of co-localization for each object, nor on the property of the co-localizing objects (such as intensity or volume) can be obtained.

Here, we first summarize the critical steps for optimized image acquisition and present a new plugin, DiAna -for Distance Analysis. This plugin allows to segment the objects as well as to perform in-depth analysis of co-localization and distance between objects. The applicability of the various tools provided by DiAna is illustrated with images of neuronal synaptic markers, since they are objects with known co-localization patterns. The analysis of those pre- and post-synaptic elements that form a synapse is representative of the sub-cellular co-localization analysis which can be performed with DiAna and can be transferred to any kind of biological structures.

## 2 Material and methods

### 2.1 Animal care

Animal care was conducted in accordance with standard ethical guidelines (NIH publication no. 85-23, revised 1985 and European Committee Guidelines on the Care and Use of Laboratory Animals 86/609/EEC), and the experiments were approved by the local ethic committee. Male mice weighing 22-24 gm were housed 5 per cage and acclimatized to laboratory conditions (12hr light/dark cycle, 21+/-1°C room temperature) with *ad libitum* access to food and water. VGLUT1-venus knock-in mice

express the Vesicular GLUtamate Transporter 1 (VGLUT1) fused to the fluorescent protein Venus under VGLUT1 endogenous promoter [15].

## 2.2 Sample preparation

Mice brains were fixed by intracardiac perfusion of 4% paraformaldehyde in 0.1 M $NA_2HPO_4/NaH_2/PO_4$ (phosphate buffer, PBS), pH 7.4. Brains were dissected and post-fixed overnight at 4 °C. Coronal sections of 50 µm thickness were cut with a vibratome (Leica).

## 2.3 Immunofluorescence

Sections were permeabilized for 30 min in PBS containing 0.1% Triton X-100 and 3% bovine serum albumin (BSA). The sections were incubated with the primary antibody in PBS with 3% BSA overnight at 4°C. The antibodies used were mouse monoclonal directed against synaptophysin (1/1000, Sigma), mouse monoclonal directed against bassoon (1/1000, Stressgene), rabbit polyclonal directed against tyrosine hydroxylase (1/1000, Sigma). Following three washing steps of 15 minutes with PBS, secondary antibody conjugated with the fluorochrome alexa-561 or alexa-488 directed against either mouse or rabbit (1/500, Invitrogen) was incubated in PBS with 3% BSA for 2 hours at room temperature. After washing, sections were rinsed before mounting in Prolong Gold.

## 2.4 Confocal image acquisition and deconvolution

Images stacks were taken with a Confocal Laser Scanning Microscope (TCS SP5, Leica Microsystems, Germany) equipped with a 1.4 NA objective (oil immersion, Leica) with pinhole aperture set to 1 Airy Unit, pixel size of 60 nm and z-step of 200 nm. Excitation wavelength was 488, 514 or 561, and emission range was 500-550, 525-540 or 570-620 nm, for detection of alexa-488, venus or alexa-561, respectively. Laser intensity and photomultiplier tube gain were set so the image occupies the full dynamic range of the detector. Deconvolution was performed using an experimental Point Spread Function obtained from fluorescent beads and Maximum Likelihood Estimation algorithm (Huygens software, Scientific Volume Imaging, Netherlands). 150 iterations were applied in classical mode, background intensity was averaged from the voxels with lowest intensity, and signal to noise ratio values were set to a value of 15.

## 2.5 Segmentation

Three segmentation procedures are implemented in the plugin. The first one is global intensity thresholding of the image. The second one is based on spot segmentation [16]. Local maxima are computed in the image, and a user-defined threshold allows selecting the local maxima belonging to objects. Then the 3D radial distribution of the voxel intensities around each local maximum is computed and a threshold is estimated for the border of each object. When the border intensity threshold has been found, the voxels around the local maximum are examined and successively included in the segmented object through the following algorithm: each 3D neighbour voxel is examined and included in the object if 1: their intensity is above the threshold 2: if their intensity is lower than the voxel previously added to the object 3: if the other neighbours would be added to the object as well.  The third segmentation procedure is based on an iterative thresholding process, it is a simplified version of the algorithm published by Gul-Mohammed et al [17], and is based on the idea of max-trees and MSER technique [18][19]. An interval of volumes is fixed and the image will undergo thresholding at each possible threshold and segmented objects having a volume in the defined range will be extracted from the image. The extracted objects are then organized into a hierarchy. Since a same object can be extracted with different thresholds, the corresponding extracted objects will be stored in different branches of the hierarchy. In case an object will split into two objects at higher threshold, a branch division will be created. Then on all final branches, corresponding to higher thresholds, the thresholds yielding to most stable objects, in term of volume, will be computed and the corresponding object will be displayed as the best object on this branch, all other instances of this object will then be discarded.

Unless stated differently, segmentation was performed in 3D using the spot segmentation procedure using the following parameters: Maxima detection: radius in xy-axis=4, in z-axis=3, noise parameter set to zero; Threshold for maxima selection was set to 5000; Parameters for Gaussian fit and threshold calculation were Radius maximum=10, S.D. value=1.5.

The validation of the segmentation was estimated by calculation of F-measure. The accuracy was classically measured by F = 2 * (Precision * Recall) / (Precision + Recall). Precision and Recall are estimates of false positives and false negatives rate, respectively.

## 2.6 Distance analysis

Distance analyses are based on classical euclidean distance computation. We implemented centre-to-centre distances, centre-to-edge distances and edge-to-edge distances. In order to be computationally efficient the objects are defined as the list of the voxels comprising the object. For edge-to-edge distance analysis, the list of contour voxels are extracted and put into a KD-tree for efficient distance computation [20]. The edge-to-edge distance is hence the smallest distance between the two objects, and will be equal to 0 if the two objects intersect. The closest objects are also computed using a KD-tree approach for efficiency.

### 2.7 Co-localization and contact surface analysis

The computation of co-localized voxels is based on the analysis of the corresponding labeled images of the objects [21]. The object 1 is labeled with values 1 in the first image and the object 2 with values 2 in the second image, the two images are then summed up. The number of voxels having a value 3 will hence correspond to the number of co-localized voxels between the two objects. From two non-co-localized objects we implemented a contact surface computation. We define a minimum distance between the borders of the two objects and compute the number of border voxels from one object having border voxels from the other object below the defined distance.

### 2.8 Statistical computation

In order to compute robust co-localization analysis, we need to assess the statistical significance of the co-localization. Based on the idea of the randomization of pixels described by Costes, we carry out a randomization of object's positions. A new position is randomly assigned to the objects, while ensuring the objects remain in the surrounding structure and do not intersect with other objects. Based on this randomization we used the framework defined by Andrey et al [22] to define an index describing the statistical significance of the co-localization. We first compute the cumulated distribution function (cdf) of all distances between the centres of objects of the first channel to the centre of the closest object in the second channel for the observed data. We then compute the same cdf for $n$ randomized data and rank the observed data among the $n$ randomized data. For a 5% interval, if the observed data falls into the first or last 2.5% of the randomized data, we can then reject the hypothesis than the co-localization is only due to chance, as this may happen in high density objects populations.

7

### 3 Results and discussion

#### 3.1 Segmentation: Determination of the objects in the image

Segmentation is a process that allows the identification of objects in digital images. Binarization assigns a value of either 0 or 1 to each pixel. Pixels belonging to objects have a value of 1, background pixels have a value of 0. In a second step, the objects are labelled, which means that all neighbouring pixels with a value of 1 are grouped to define an object. Segmentation is thus a process by which a gray-scale image becomes a space in which objects are located. In the most classical segmentation procedure, an intensity threshold is used to binarize the image. Before thresholding, smoothing of the image with an appropriate filter can be performed with the plugin DiAna, if the image has previously not been deconvolved and noise filtered. Indeed, proper image acquisition and pre-processing facilitates subsequent object extraction by image segmentation for reliable analysis. The preparation of the sample and image acquisition have been extensively discussed elsewhere [5][23][24][25], and the benefits of deconvolution have been well demonstrated [23][26][27][28] Noise filtering and global thresholding are implemented in DiAna, so objects can be extracted before analysis. The major problem with intensity thresholding lies in the fact that this is a global approach. If the image contains bright and faint objects, the application of a single threshold to the image will end with the bright objects being too big or the faint objects being too small. Hence, a local approach for segmentation is often more useful. Therefore, we included two 3D segmentation procedures in the DiAna plugin, which allow for segmentation of image containing objects with different sizes and intensities (Fig. 1). The "spot segmentation" procedure is based on detection of objects with local maxima and 3D analysis of the intensity distribution around the maxima [16] (Fig. 1A,B). This procedure brings the advantage that objects with different intensities will be properly segmented. It should, however, be noted that each local maximum is a seed that marks an object, it is thus advised to deconvolve or apply smoothing filters before maxima detection, and to carefully set the intensity threshold for maxima selection. The plugin DiAna offers visualization the local maxima so best parameters can be found before performing segmentation. Finally, it is noteworthy that the method is best suited for spot-like objects since in case of irregular objects several local maxima may be found within the same object which would then be split. Therefore, we introduced a tool in the ROI manager for manually selecting and merging pairs of objects when necessary. The "iterative segmentation"

8

procedure extracts each object by examining the output of thresholding at different intensity values [17] (Fig. 1C). A complete version of these segmentation procedures with more options can be found in the 3D Image Suite [29][30].

The segmentation procedures implemented in DiAna were validated for an image of neuronal presynaptic elements by immunofluorescence labelling of tyrosine hydroxylase, acquired with confocal microscopy (Supplementary Fig. S1). In comparison to the ground truth (positive objects eye counted by experimenter), both segmentation procedures extracted objects accurately (F-measure of 0.992 and 0.987 for spot and iterative procedure, respectively). The output of segmentation was further tested on another dataset from similar objects to compare results from raw and deconvolved image. The segmentation was less precise on raw images but still efficient enough to apply co-localization analysis (F-measure for deconvolved images 0.966 and 1, and for raw images 0.934 and 0.966, for spot and iterative procedure, respectively). The algorithms in both spot and iterative segmentation procedures have been chosen so they are generally applicable to most biological images with good robustness. However, users are advised to test several values for the parameters and validate the segmentation by visual inspection of the segmentation result. It is a general rule that only the biologist can properly estimate whether the segmented objects correspond to what he/she considers as biological objects. Images of similar biological objects often contain variable intensities. This may be due to differences in the efficacy of fluorescent labelling from one experiment to another, or from lack of stability of the excitation and detection system of the microscope. Therefore, the values determined for the parameters of the segmentation may not be applicable to two different sets of images. A way to circumvent this problem is to normalize the mean intensity of the whole image [23] before defining the segmentation parameters and reliably applying them to all images of the study.

### 3.2 Three-dimensional measurements for object analysis

Following the application of the segmentation procedure described in section 3.1, DiAna offers precise 3D measurements for co-localization and distance analysis. Of note, users can segment their images with any other method of their choice and directly use the analysis tools of DiAna. The plugin quantifies several parameters for pairs of objects (Fig. 2). It also introduces measurement of surface of contact for distant and co-localizing objects, which requires a user-defined edge-to-edge distance (Fig. 2E). Those parameters are used for co-localization and distance analysis as described in sections 3.3

and 3.4. Moreover, DiAna performs measurements of several parameters such as volume, mean intensities, surface area, Feret's diameter, coordinates of centers of mass and centroids for all objects of the image.

### 3.3 Co-localization analysis with DiAna

Co-localization is determined by the detection of overlapping objects. DiAna computes distances between co-localizing objects (Fig. 2A-C) as well as measurements of co-localizing object volumes for each pair of objects (Fig. 2D). Those measurements allow for precise quantification of the co-localization. Figure 3 shows two biological examples where images of synaptic markers with known differences in co-localization where analysed with DiAna. Note that some spots are excluded from segmentation because they are not biologically relevant. VGLUT1 can sparsely be found in the axon in between the presynaptic elements which are the objects to be extracted [31] and immunofluorescence for synaptophysin and bassoon retrieves low intensity background besides relevant signal. The co-localization of the vesicular transporter VGLUT1 with synaptophysin (Fig. 3A) and with Bassoon (Fig. 3B) was analysed by determining centre-to-centre distances and the percentage of the co-localization volume (Fig. 3C,D). A perfect co-localization between VGLUT1 and synaptophysin was revealed with a centre-to-centre distance smaller than optical resolution, while the co-localization between VGLUT1 and bassoon is not complete, as shown by a longer centre-to-centre distance and lower percentage of co-localization for each pair of objects. Those results fit the measurements performed from electron microscopy and STED microscopy data [32][33], as VGLUT1 and synaptophysin are found in the main vesicular pool while bassoon is restricted to the active zone next to the plasma membrane of the presynapse [34][35].

Interestingly, the percentage of the co-localizing object's volume given by DiAna allows using a cut-off to discard false positives, which could appear because the blur in z-axis can lead to small overlap between objects (Fig. 3E). This loss of axial resolution can be reduced by refractive index matching [36] and by deconvolution [27][28]. It is noteworthy that it was measured that deconvolution improves co-localization analysis [37][38][39].

Finally, in addition to co-localization measurements, DiAna retrieves tables with quantifications such as volume and mean intensity for each object of both images. Each object is identified in the co-

10

localization and measurement's tables, ensuring that a correlation between chosen criteria can be drawn.

### 3.4 Distance analysis with DiAna

DiAna also offers a distance analysis for either co-localized objects or for all objects from the two images. For each object from one image, the centre to centre distances with all objects of the other image are computed in 3D. By default, the plugin identifies the closest, not co-localizing, object. The user can also select the rank of the objects to be included in the result table (first closest only, first and second closest, first to fifth etc.). Note that in this case the co-localizing objects will be included in the results as the first closest objects. The distances measured can be used to plot a histogram of distances between neighbouring objects for spatial distribution analysis, and correlation between quantified parameters from the object pair can be assessed. Figure 4 shows the spatial analysis in a biological example where the distances of two synaptic markers, the vesicular transporter VGLUT1 and tyrosine hydroxylase where analysed with DiAna. The analysis of the distances to the first closest object shows that objects from the red channel are preferentially localized in the vicinity of objects from the green channel, since 50% of all red objects are found in a distance below 1 micron to a green object, which exactly fits with measurements performed on images obtained by electron microscopy [40].

The distance analysis can furthermore be used to assess co-localization in the case where objects are represented as single voxels. DiAna can be used to estimate co-localization from images of the centre of the objects. The centre-to-centre distance, given by the distance analysis, allows determination which objects do co-localize (Fig. 5). The measured distances can be ranked to set a threshold value, which will define which single-voxel objects do co-localize. Co-localization can be decided if the distance is smaller than the optical resolution. In this case the threshold distance can be either set to zero or more, depending on the resolution of the image (Fig. 5A-C). Alternatively, the co-localization can be decided if the distance value is lower than a threshold distance estimated on the basis of the knowledge of minimal size of the objects (Fig. 5A,D). It is noteworthy that this method can be applied for co-localization analysis in images of single particles, in which objects are represented as single voxels, often identified as the peak of the Gaussian distribution of objects intensity.

### 3.5 Assessing statistical robustness in object based co-localization analysis

In pixel-based co-localization analysis, statistical significance of co-localization may be estimated by comparing co-localization measurements before and after randomization of pixels. Costes et al. [10] confronted the Pearson coefficient (PC) of an image pair with correlation coefficients obtained between the green channel and randomized images of the red channel. To do so, they shuffled pixel blocks of one fluorescent channel in a randomized manner and measured the PC after each randomization round. They obtained a Gaussian distribution of PC after randomization and deduced that the PC obtained for the original image pair would be statistically significant if it is not included in the area of the Gaussian curve. With the DiAna plugin, we introduce a similar method, originating from spatial statistics analysis and described in Andrey et al 2010 [22], applied to object-based co-localization (Fig. 6). First, objects from one image are randomly redistributed. The shuffle function allows to either redistribute the objects in a uniform manner within the whole image, or to import a binary image which defines regions in which redistribution is constrained (Fig. 6A-C). Shuffled images are generated, and for each of these images the centre-to-centre distances between objects of the randomized channel to the closest object in the second channel from the original image are computed. The cumulative distribution of the distances is plotted, and represented as the mean (Fig. 6D, red curves) flanked by 95% confidence intervals of the results (Fig. 6D, green curves). In parallel, observed centre-to-centre distances between objects from the non-randomised original images are measured and plotted on the same graphic (Fig. 6D, blue curves). Statistical significance is assessed by the null hypothesis that the experimental data are due to randomness. If the distribution of the distances from experimental images falls outside the confidence interval of the distance distribution obtained for shuffled images in which object locations are random, one concludes that there is less than 5% chance ($p<0.05$) that the observed distribution is random and thus the co-localization is considered as statistically significant. In addition, the plugin calculates the rank of the observed distribution within $n$ distributions obtained from shuffled images. A rank lower than 0.025 or higher than 0.975 indicates that the probability that the observed distribution is random is inferior to 5 % and the co-localization is then considered significant. In the example of the figure 6, the co-localization of VGLUT1 and synaptophysin was assessed and the analysis shows that the co-localization is significant, which is expected as these two proteins are both found in the vesicles from the presynaptic element of neurons [35][41].

Note that this methodology for assessing statistical robustness using a randomization procedure is quite generic and can be applied to other functions for co-localization analysis and generally to many other problems.

**4 Conclusion**

We have developed an ImageJ-based tool named DiAna, allowing for spatial analysis in the three dimensions. In this tool we implemented two methods of 3D-segmentation, which show faithful and robust object extraction despite high variability of object size and intensity within the image. Furthermore, the tool allows executing extended object-based co-localization and distance analysis between objects in 3D. After co-localization or distance analysis, quantifications for each object are possible. Finally, we introduce a new method for the estimation of statistical significance of object-based co-localization. The algorithms we developed are implemented in a user-friendly plugin, which allows for complete but intuitive 3D image analysis, applicable to a large variety of biological objects. The plugin with instructions for use can be found at [http://imagejdocu.tudor.lu/doku.php?id=plugin:analysis:distance_analysis_diana_2d_3d_:start].

**References**

[1] Q. Li, A. Lau, T.J. Morris, L. Guo, C.B. Fordyce, E.F. Stanley, A syntaxin 1, Galphao, and N-type calcium channel complex at a presynaptic nerve terminal: analysis by quantitative immunocolocalization, J. Neurosci. 24 (2004) 4070–4081.

[2] E. Manders, J. Stap, G. Brakenhoff, R. Van Driel, J. Aten, Dynamics of three-dimensional replication patterns during the S-phase, analysed by double labelling of DNA and confocal microscopy, J. Cell Sci. 103 (1992) 857–862.

[3] E. Lachmanovich,D. E Shvartsman, Y. Malka, C. Botvin, Y.I. Henis, A.M. Weiss, Co-localization analysis of complex formation among membrane proteins by computerized fluorescence microscopy: application to immunofluorescence co-patching studies, J. Microsc. 212 (2003) 122–131.

[4] B. Obara, A. Jabeen, N. Fernandez, P.P. Laissue, A novel method for quantified, superresolved, three-dimensional colocalisation of isotropic, fluorescent particles, Histochem Cell Biol 139 (2013) 391-402.

[5] S. Bolte and F.P. Cordelieres, A guided tour into subcellular colocalization analysis in light microscopy, J. Microsc. 224 (2006) 213-232.

[6] F. Jaskolski, C. Mulle, O.J. Manzoni, An automated method to quantify and visualize colocalized fluorescent signals, J. Neurosci. Meth. 146 (2006) 42–49.

[7] F.P. Cordelières, S. Bolte, Experimenters' guide to co-localization studies: finding a way through indicators and quantifiers, in practice, Methods in Cell Biology 123 (2014) ISSN 0091-679X, chapter 21.

[8] T. Lagache, N.Sauvonnet, L. Danglot, J.C. Olivo-Marin, Statistical analysis of molecule colocalization in bioimaging, Cytometry A 87 (2015) 568-579.

[9] E. Manders, A. Visser, A. Koppen, W. De Leeuw, R. Van Liere, G. Brakenhoff, R. Van Driel, Four-dimensional imaging of chromatin dynamics during the assembly of the interphase nucleus, Chromosome Res 11 (2003) 537–547.

[10] S.V. Costes, D. Daelemans, E.H. Cho, Z. Dobbin, G. Pavlakis, S. Lockett, Automatic and quantitative measurement of protein-protein colocalization in live cells, Biophys. J. 86 (2004) 3993–4003.

[11] B. Van Steensel, E. Van Binnendijk, C. Hornsby, H. Van Der Voort, Z. Krozowski, E. De Kloet, R. Van Driel, Partial colocalization of glucocorticoid and mineralocorticoid receptors in discrete compartments in nuclei of rat hippocampus neurons, J. Cell Sci. 109 (1996) 787–792.

[12] E. Meijering, Cell segmentation: 50 years down the road, IEEE Signal Processing Magazine 29 (2012) 140-145.

[13] V. Wiesmann, D. Franz, C. Held, C. Münzenmayer, R. Palmisano, T. Wittenberg T, Review of free software tools for image analysis of fluorescence cell micrographs, J Microsc. 257 (2015) 39-53.

[14] T. Lagache, V. Meas-Yedid, J.C. Olivo-Marin, A statistical analysis of spatial colocalization using ripley's k function, IEEE International Symposium on Biomedical Imaging ISBI, San Francisco, 2013. pp 896–901.

[15] E. Herzog, F. Nadrigny, K. Silm, C. Biesemann, I. Helling, T. Bersot, H. Steffens, R. Schwartzmann, U.V. Nägerl, S. El Mestikawy, J. Rhee, F. Kirchhoff, N. Brose, In vivo imaging of intersynaptic vesicle exchange using VGLUT1 Venus knock-in mice, J Neurosci 26 (2011) 15544-15559.

[16] N. Heck, M. Dos Santos, B. Amairi, M. Salery, A. Besnard, E. Herzog, T. Boudier, P. Vanhoutte, J. Caboche, A new automated 3D detection of synaptic contacts reveals the formation of cortico-striatal synapses upon cocaine treatment in vivo, Brain Struct Funct 220(2015) 2953-2966.

[17] J. Gul-Mohammed, I. Arganda-Carreras, P. Andrey, V. Galy, T. Boudier, A generic classification-based method for segmentation of nuclei in 3D images of early embryos, BMC Bioinformatics 14 (2014) 15-19.

[18] J. Matas, O. Chum, M. Urban, T. Pajdla, Robust wide-baseline stereo from maximally stable extremal regions, Image and vision computing 22 (2004) 761-767

[19] L.A. Tavares, R.M. Souza, L. Rittner, R.C. Machado, R.A. Lotufo, Interactive max-tree visualization tool image processing and analysis, Image Processing Theory, Tools and Applications (2015) Conference article 119-124.

[20] J.L. Bentley, Multidimensional binary search tree used for associative searching, Communications of the ACM 18 (1975) 509-517.

[21] D.A. Randell, G. Landini, A. Galton, Discrete Mereotopology for spatial reasoning in automated histological image analysis, *IEEE Trans Patt Rec Mach Intell* 35(2013) 568-581.

[22] Andrey P, Kiêu K, Kress C, Lehmann G, Tirichine L, Liu Z, Biot E, Adenot PG, Hue-Beauvais C, Houba-Hérin N, Duranthon V, Devinoy E, Beaujean N, Gaudin V, Maurin Y, Debey P. Statistical analysis of 3D images detects regular spatial distributions of centromeres and chromocenters in animal and plant nuclei. PLoS Comput Biol. 2010 Jul 8;6(7):e1000853.

[23] O. Ronneberger, D. Baddeley, F. Scheipl, P.J. Verveer, H. Burkhardt, C. Cremer, L. Fahrmeir, T. Cremer, B. Joffe, Spatial quantitative analysis of fluorescently labeled nuclear structures: problems, methods, pitfalls, Chromosome Res 16 (2008) 523-562.

[24] A.J. North, Seeing is believing? A beginners' guide to practical pitfalls in image acquisition, J Cell Biol. 172 (2006) 9-18.

[25] J.W. Lichtman, J.A. Conchello, Fluorescence microscopy, Nat Methods 12 (2005) 910-919.

[26] N. Heck, S. Betuing, P. Vanhoutte, J. Caboche, A deconvolution method to improve automated 3D-analysis of dendritic spines: application to a mouse model of Huntington's disease, Brain Struct Funct 217(2012) 421-434.

[27] J.G. McNally, T. Karpova, J. Cooper, J.A. Conchello, Threedimensional imaging by deconvolution microscopy, Methods 19 (1999) 373–385.

[28] W. Wallace, L. Schaefer, J. Swedlow,  A workingperson's guide to deconvolution in light microscopy, BioTechniques 31 (2001) 1076-1097.

[29] J. Ollion, J. Cochennec, F. Loll, C. Escudé, T. Boudier, TANGO: A Generic Tool for High-throughput 3D Image Analysis for Studying Nuclear Organization. Bioinformatics 29 (2013) 1840-1841.

[30] http://imagejdocu.tudor.lu/doku.php?id=plugin:stacks:3d_ij_suite:start

[31] K. Staras, T. Branco, J.J. Burden, K. Pozo, K. Darcy, V. Marra, A. Ratnayaka, Y. Goda, A vesicle superpool spans multiple presynaptic terminals in hippocampal neurons, Neuron 66 (2010) 37-44.

[32] C. Kempf, T. Staudt, P. Bingen, H. Horstmann, J. Engelhardt, S.W. Hell, T. Kuner, Tissue multicolor STED nanoscopy of presynaptic proteins in the calyx of Held, PLoS One 8 (2013) e62893.

[33] C.C. Garner, S. Kindler, E.D. Gundelfinger, Molecular determinants of presynaptic active zones, Curr Opin Neurobiol. 10 (2000) 321-327.

[34] F.E. Schweizer, T.A. Ryan, The synaptic vesicle: cycle of exocytosis and endocytosis, Curr Opin Neurobiol. 16 (2006) 298-304.

[35] T.C. Südhof, R. Jahn, Proteins of synaptic vesicles involved in exocytosis and membrane recycling, Neuron 6 (1991) 665-677.

[36] C. Fouquet, J.F. Gilles, N. Heck, M. Dos Santos, R. Schwartzmann, V. Cannaya, M.P. Morel, R.S. Davidson, A. Trembleau, S. Bolte, Improving axial resolution in confocal microscopy with new high refractive index mounting media, PLoS One, 10 (2015):e0121096.

[37] L. Landmann, P. Marbet, Colocalization analysis yields superior results after image restoration, Microsc Res Tech 64 (2004) 103-112.

[38] L. Landmann, Deconvolution improves colocalization analysis of multiple fluorochromes in 3D confocal data sets more than filtering techniques, J Microsc 208(2002) 134-147.

[39] T. Abraham, S.E. Allan, M.K. Levings, Deconvolution and chromatic aberration corrections in quantifying colocalization of a transcription factor in three-dimensional cellular space, Micron. 41(2010) 633-640.

[40] J. Moss, J.P. Bolam, A dopaminergic axon lattice in the striatum and its relationship with cortical and thalamic terminals, J Neurosci. 28 (2008) 11221-11230.

[41] M. Grønborg, N.J. Pavlos, I. Brunk, J.J. Chua, A. Münster-Wandowski, D. Riedel, G. Ahnert-Hilger, H. Urlaub, R. Jahn, Quantitative comparison of glutamatergic and GABAergic synaptic vesicles unveils selectivity for few proteins including MAL2, a novel synaptic vesicle protein, J Neurosci. 30 (2010) 2-12.

**Figure legends**

**Figure 1. Principles of the segmentation procedures performed by the plugin DiAna**

A. Detection of local maxima for segmentation of the objects with the spot segmentation procedure.

A1. In noisy images, the "noise" parameter allows the local maxima outside the objects to be discarded. For the radius parameter, a low radius (2x2) retrieves several maxima within the same object. A bigger radius (3x3) ensures minimal distance between local maxima and avoids this problem. An example is encircled in red.

A2. The maxima detection is more robust in deconvolved or properly noise-filtered images.

A3. Prior segmentation, a user-defined threshold intensity value allows selecting the maxima belonging to the objects.

A4. Result of the spot segmentation further explained in B.

B. Workflow of the spot segmentation procedure. B1. Maxima are detected as shown in A. B2. 3D radial distribution of the intensity centred to the maxima is computed. The user should define a maximum value in voxel for the radius of the largest sphere. It is advised that it is bigger than the largest object expected in the image.  B3. The distribution is plotted and fitted to a Gaussian curve. The user defines a factor applied to the standard deviation of the Gaussian curve, which sets the size of a horizontal line placed to cover the area defined by the Gaussian curve (i.e. the size of the object). Factors of 1.5 and 2 will cover 86.6 and 95.4% of the Gaussian curve, respectively. The corresponding intensity value on y-axis of the graphic is the threshold used for segmentation of the object. B4. The procedure allows finding a specific threshold for objects of different intensities. Voxels around the maxima are successively included in the segmented object through an algorithm with three criteria of acceptance: The first criterion is that the voxel intensity should be higher than the defined threshold. The second criterion is that their intensity should be lower than the intensity of the voxels previously included in the objects, which avoids merging of adjacent objects as shown in B5. The third criterion is that the voxel is included on the condition that neighbouring voxels are included as well, which avoids creation of filamentous structures extruding from the object as shown in B6.

19

C. Workflow of the iterative segmentation method. C1. The image is segmented with different intensity thresholds. From low to high intensity thresholds, the objects become isolated and decrease in size. The segmented objects which fall in the volume interval defined by the user are stored in a hierarchy. C2. The selected objects are classified in a hierarchy showing the object separation and decrease in size along increasing threshold values. When an object becomes isolated it is stored in a new branch in the hierarchy. The final branches contain most disconnected objects, still having their volume in the specified interval. The best thresholds within the last branches are found with the maximum stable volume algorithm. The difference in the object volume between each threshold is computed and the threshold corresponding to the minimum difference is retained. C3. The iterative method determines a threshold specific to each object and reconstructs the segmented image.

**Figure 2. Measurements performed in DiAna plugin**

A-C. Distance analysis measurements performed by DiAna are centre-to-centre (A), edge-to-edge (B), centre-to-edge (C).

D. Percentage of co-localizing volumes normalized to the volume of either one or both objects are computed by DiAna.

E. Contact surface measurements for overlapping and distant objects. The user-defined maximum distance between objects (blue arrows) set the extent of the object contour for which the contact is defined.

**Figure 3. Detailed co-localization measurements using the plugin DiAna**

A-B. Close-ups of single sections from deconvolved and segmented image stacks showing two fluorescent channels. Images were obtained from brain sections immunolabeled for synaptic proteins (green: vesicular transporter VGLUT1, red in A: bassoon, red in B: synaptophysin).

C. Distance measurements between centres of co-localizing objects reveal that the co-localized objects from image B are closer to each other than the co-localized objects from image A.

D. Measurements of the percentage of the co-localizing volume for each object's pair reveal that the co-localizing volume is bigger for the objects from image B than for the objects from image A.

E. 3D volume rendering from image stack showing an example of co-localization artefact due to optical smear. The percentage co-localization volume is lower than 5% and a cut-off can be defined to avoid such false positives.

Images were segmented using spot segmentation protocol. Co-localization analysis was performed on image stacks containing more than 5000 objects in each channel. Scale bars in A-B: 1 micron. Note that some spots are excluded from segmentation as they are not biologically relevant.

**Figure 4. Distance analysis of paired of non co-localizing objects with the plugin DiAna**

A. Close-up of a single slice from deconvolved and segmented image stack showing both channels. Images were obtained from brain sections immunolabeled for proteins expressed in different, hence not co-localizing, synaptic structures (green: vesicular transporter VGLUT1, red: tyrosine hydroxylase).

B. Distance analysis retrieves centre-to-centre distance in between all objects from green channel and their closest neighbour in red channel. The histogram of distance distribution shows that 50% of the objects from the red channel are localized at less than 1 micron from objects of green channel.

Distance analysis was performed on image stacks containing more than 3000 objects in each channel. Scale bars in A-B: 1 micron. Note that some spots are excluded from segmentation as they are not biologically relevant.

**Figure 5. Co-localization analysis based on localization of object's centres with the plugin DiAna**

A. Distance measurements between all points from two images allows the analysis of the distance distribution of objects. The coloured bars in the histogram illustrate threshold values, which can be used to define co-localization according to criteria defined in B-D.

B. Co-localization can be defined for either a zero distance or a distance equal to voxel size.

C. Co-localization can be defined for distances which are lower than the resolution of the imaging system.

D. In case the minimal size of the biological objects are known, co-localization can be defined for distances which are lower than the sum of the minimum radiuses of objects A and B.

21

Scale bars in B-D: 300 nm. Pixel size: 60 nm.

**Figure 6. Statistical significance of the object based co-localization**

A. DiAna can perform randomization of objects localization within a selected region in the image. 3D surfacing rendering of objects segmented within a mask. Each spot corresponds to an object and the mask volume appears in grey.

B. View of the same objects as in A following the application of a shuffle procedure. The positions of the objects are randomly redistributed within the corresponding mask volume.

C. 3D surface rendering of segmented objects from two images. Images were obtained from brain sections immunolabeled for synaptic proteins (green: vesicular transporter VGLUT1, red: synaptophysin). In the shuffled image, red objects are randomly redistributed. The co-localizing volumes appear in white. Note that their occurrence is lower after shuffling. Lower panels shows close-ups from the regions of the upper panel. The objects have an average diameter of 600 nm.

D. The DiAna plugin provides a graphic, which represents the cumulative distribution of the minimum centre-to-centre distances between objects from two images. The blue curve shows the distribution for the experimental images shown in B. The red curve shows the mean distribution of distances between objects from the experimental green images and from 100 red images obtained by the shuffle procedure. The green curve represents the 2.5 and 97.5% confidence intervals around the mean. The experimental curve (in blue) is localized outside the 95% confidence interval (in green) of the distance analysis done after randomization, the co-localization is thus considered as statistically significant.

**Supplementary figure S1. Validation of the segmentation procedures implemented in the plugin DiAna**
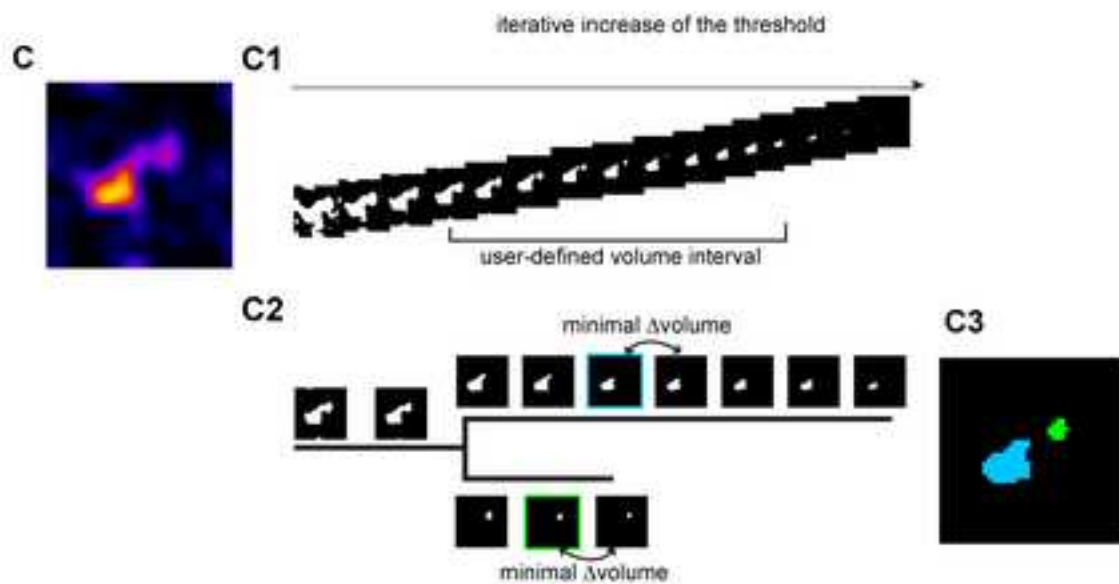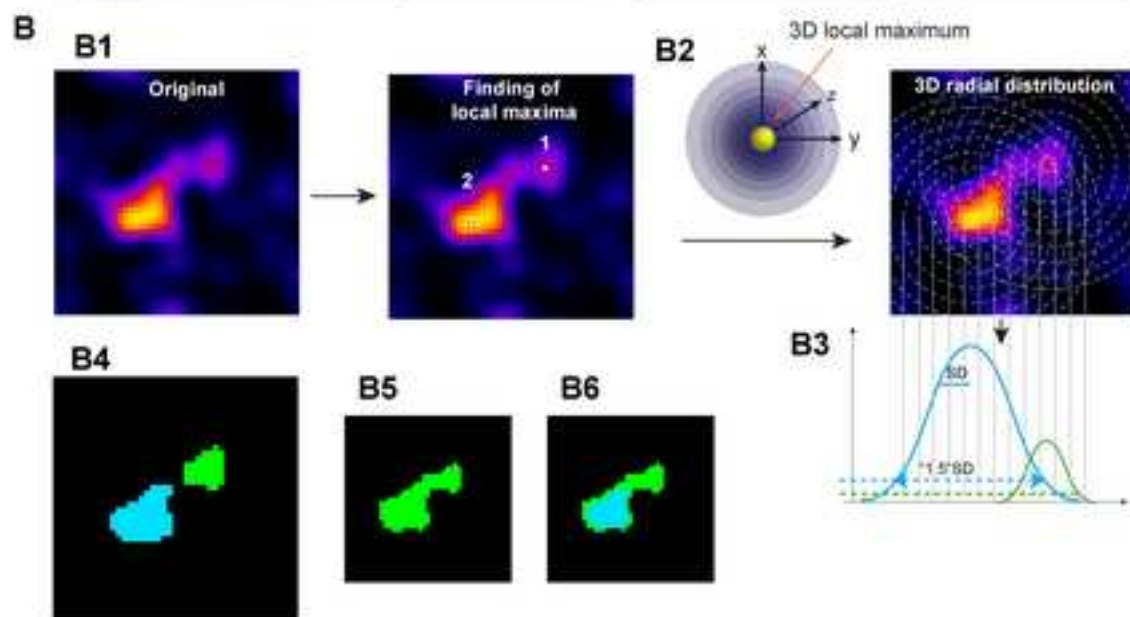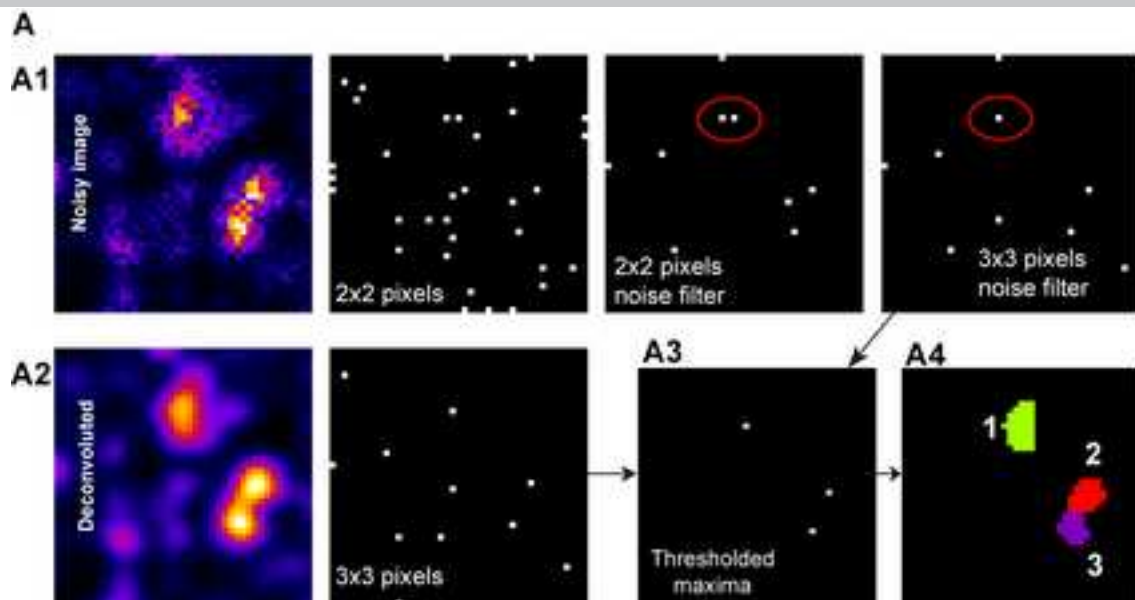
3D volume rendering of the original and segmented images are shown. In the original image, the dynamic range (intensity difference between the dimmer and the brighter object) is to too high to allow correct visualization of all objects. Images were acquired with confocal microscope on brain sections immunostained for tyrosine hydroxylase. The objects have an average diameter of 600 nm.
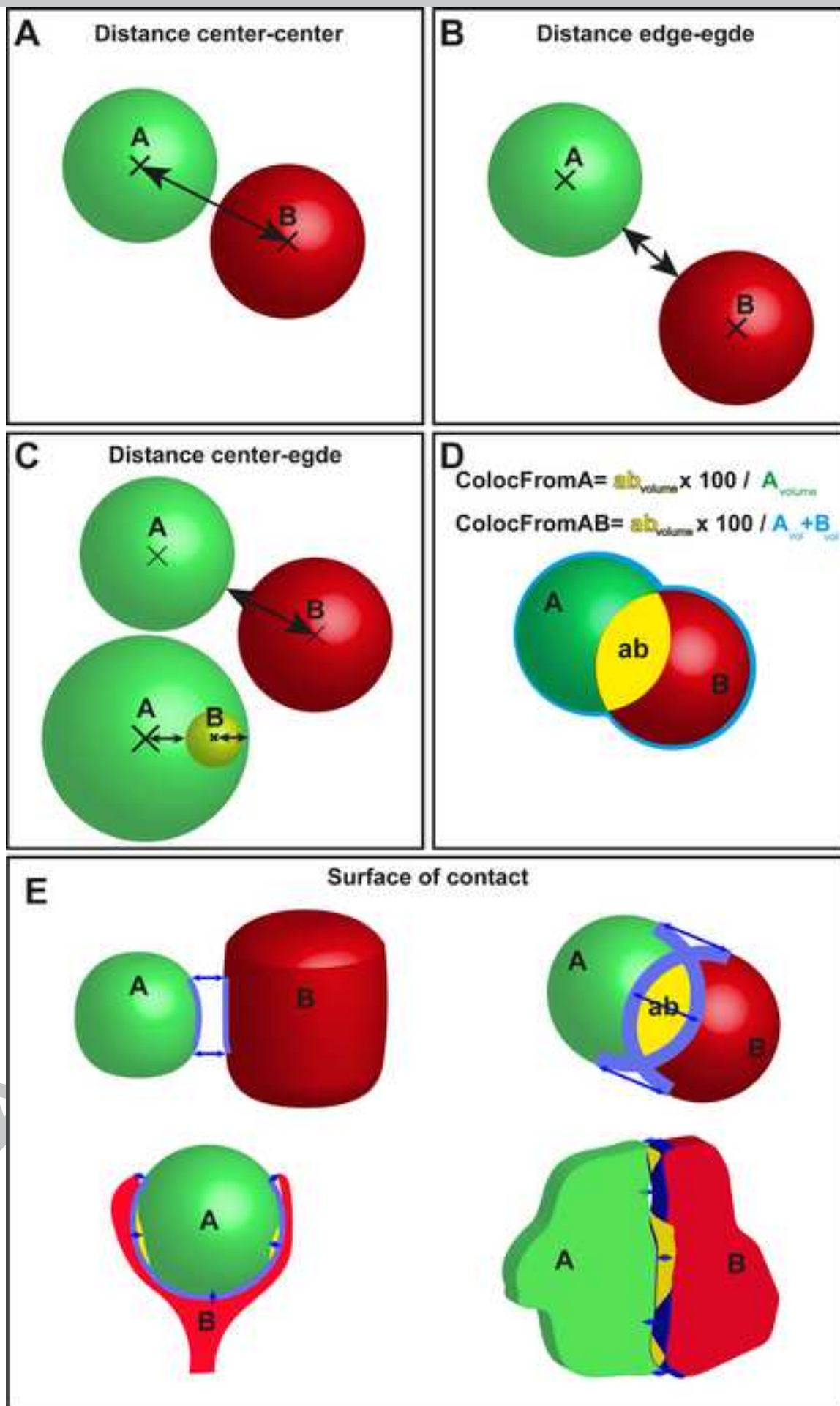
A. Manual counting by experimenter concluded for the presence of 321 objects (ground truth number of objects). The segmentation yielded 316 and 311 objects for spot and iterative procedures, respectively. Careful inspection of the images showed that 5 and 2 objects were not detected (false
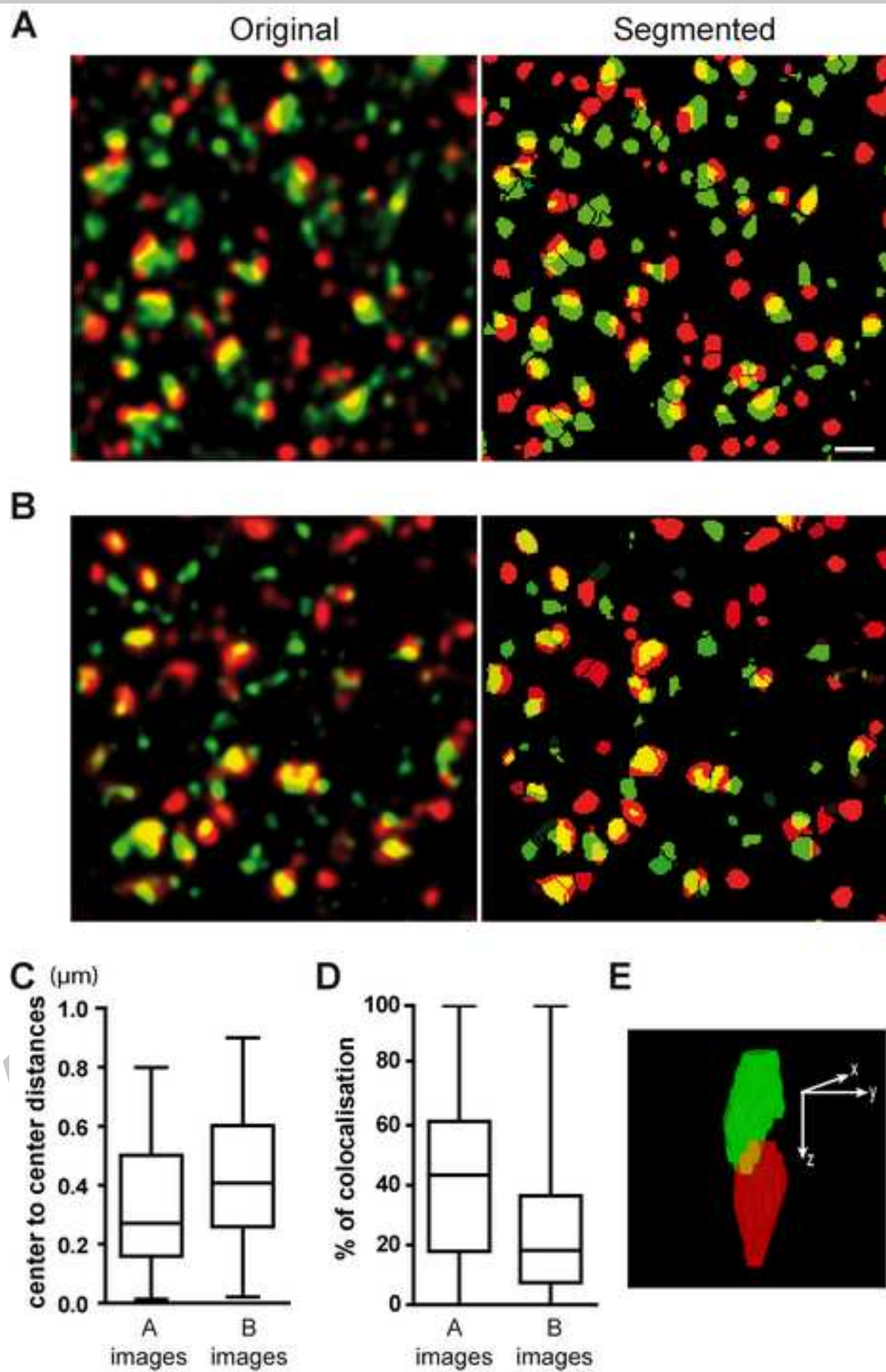
22

negative) in segmented images from the spot and iterative procedures, respectively. In addition, 7 objects in the image segmented with iterative procedure corresponded to merged spots.
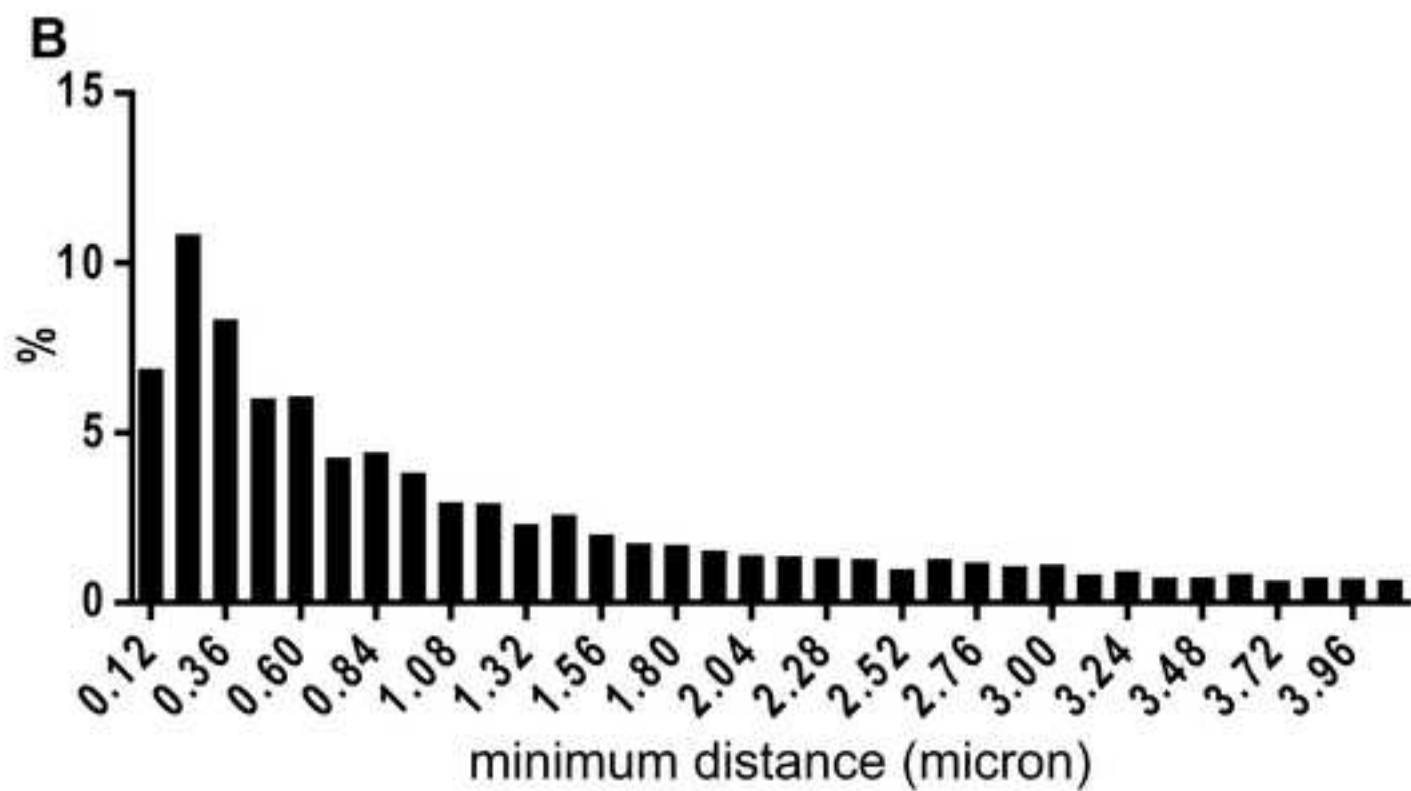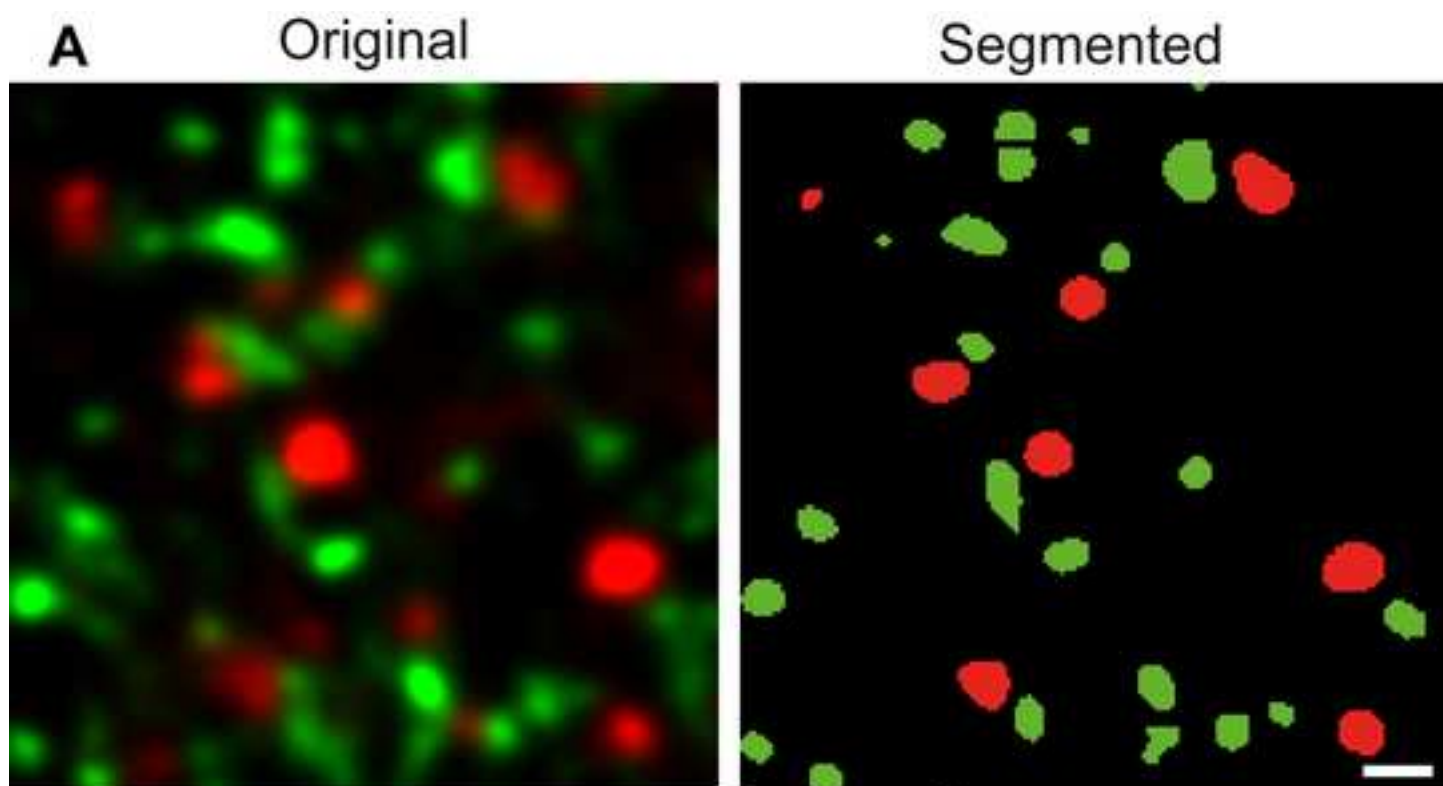
B. The output of segmentation was further tested on a smaller dataset of 57 objects to compare results from raw and deconvolved image. The spot and iterative procedures retrieved 60 and 57 objects, respectively. The 3 additional objects observed with the spot procedure were due to 3 objects wrongly split. The outcome of the segmentation for raw images was correct, but less precise than what obtained from deconvolved images. The spot segmentation on raw image gave 2 false positive and 2 false negatives. The spot segmentation gave 1 false positive, 2 false negative and 6 objects were found to be split.
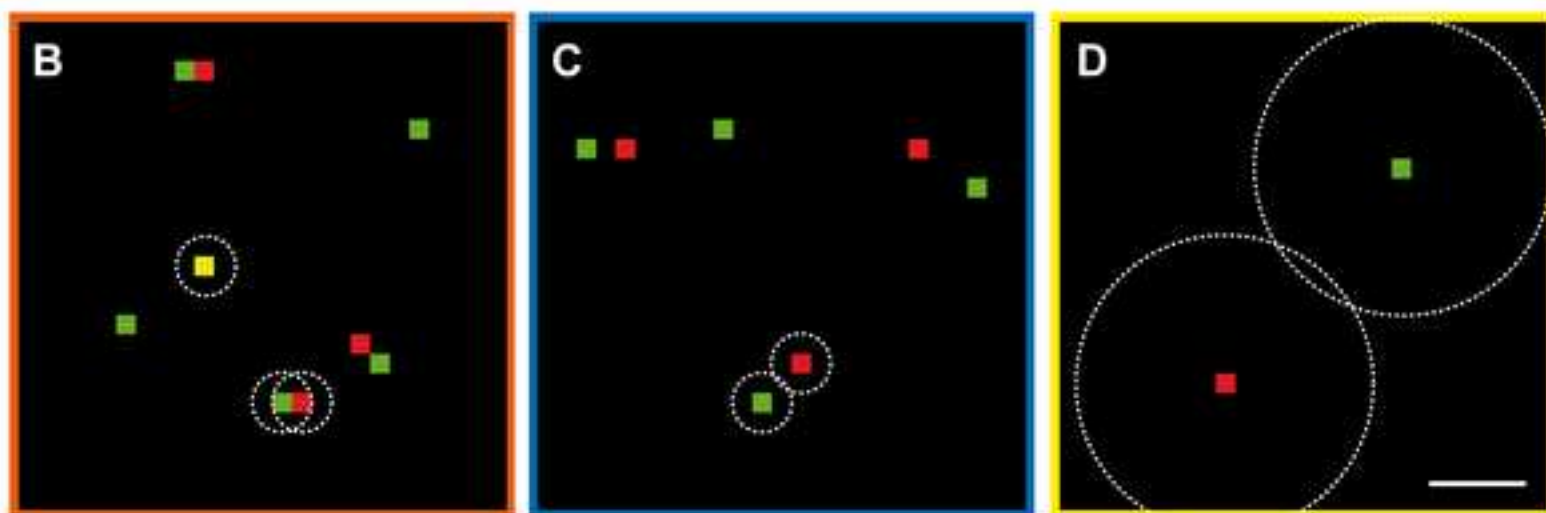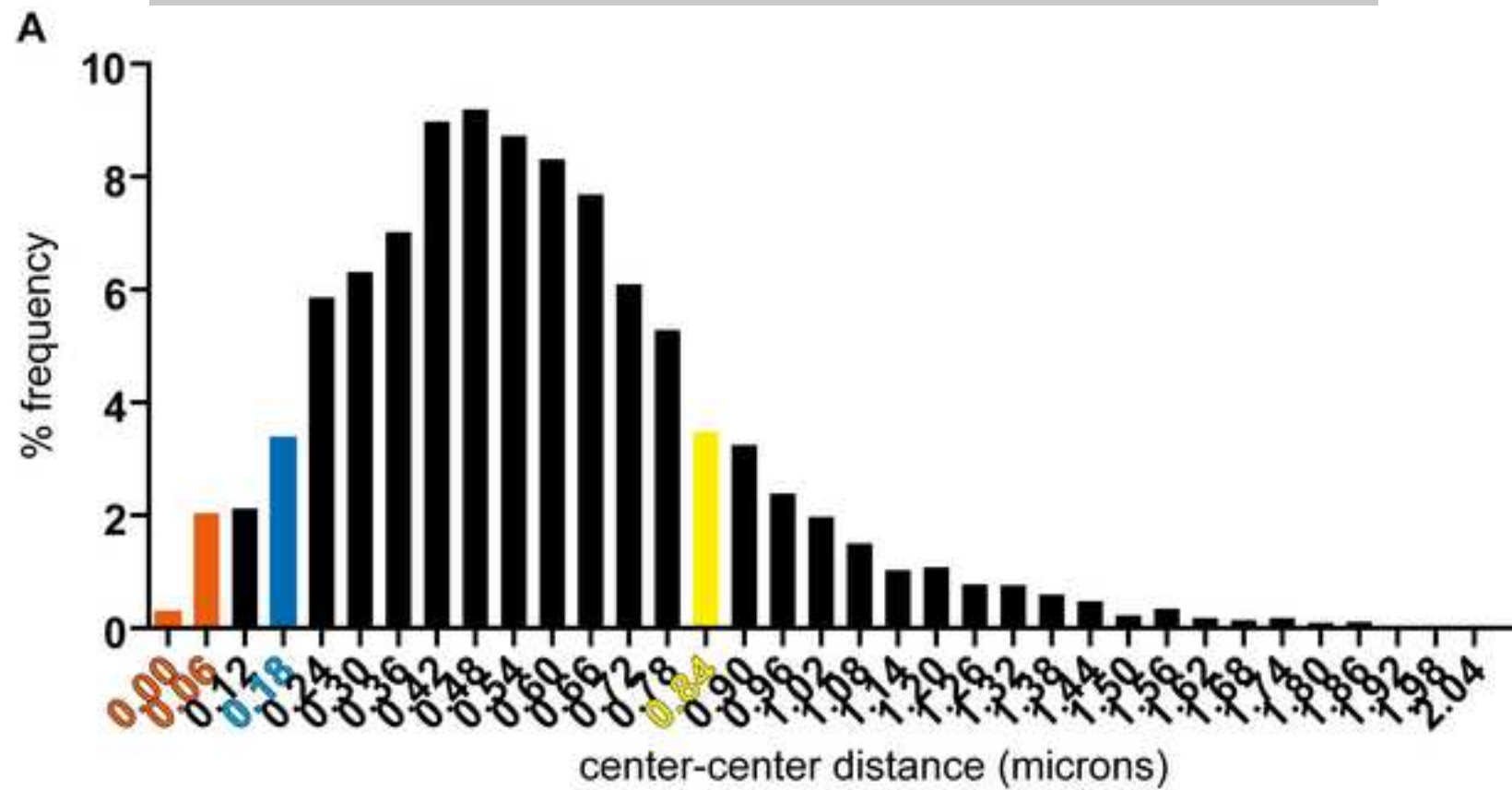
The spot segmentation was performed using the following criteria: Maxima detection: radius in xy-axis=4, in z-axis=3, noise parameter set to zero (100 for raw image); Threshold for maxima selection was set to 5000 (14000 for raw image); Parameters for Gaussian fit and threshold calculation were Radius maximum=10, S.D. value=1. The iterative segmentation was performed using the following criteria: Minimal threshold value 3000 (9000 for raw image) and a threshold interval of 500. The volume interval considered was from 27 to 1000 voxels.

**Figure1**

**Figure2**

**A** Distance center-center

**B** Distance edge-egde

**C** Distance center-egde

**D**

$$ColocFromA = ab_{volume} \times 100 \ / \ A_{volume}$$

$$ColocFromAB = ab_{volume} \times 100 \ / \ A_{vol} + B_{vol}$$

ab
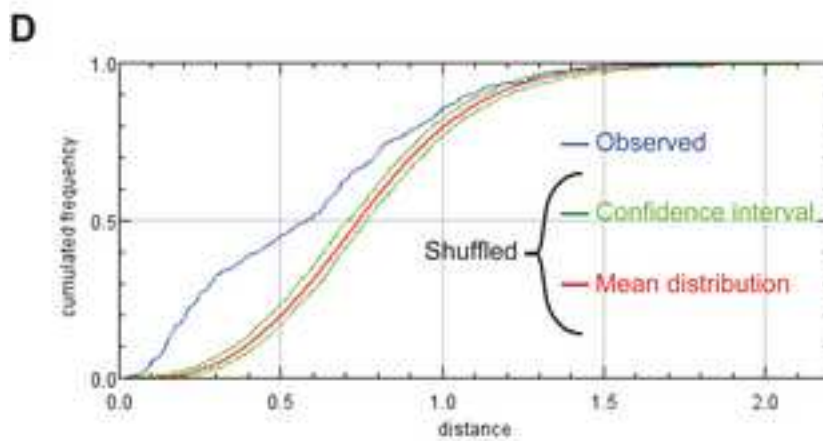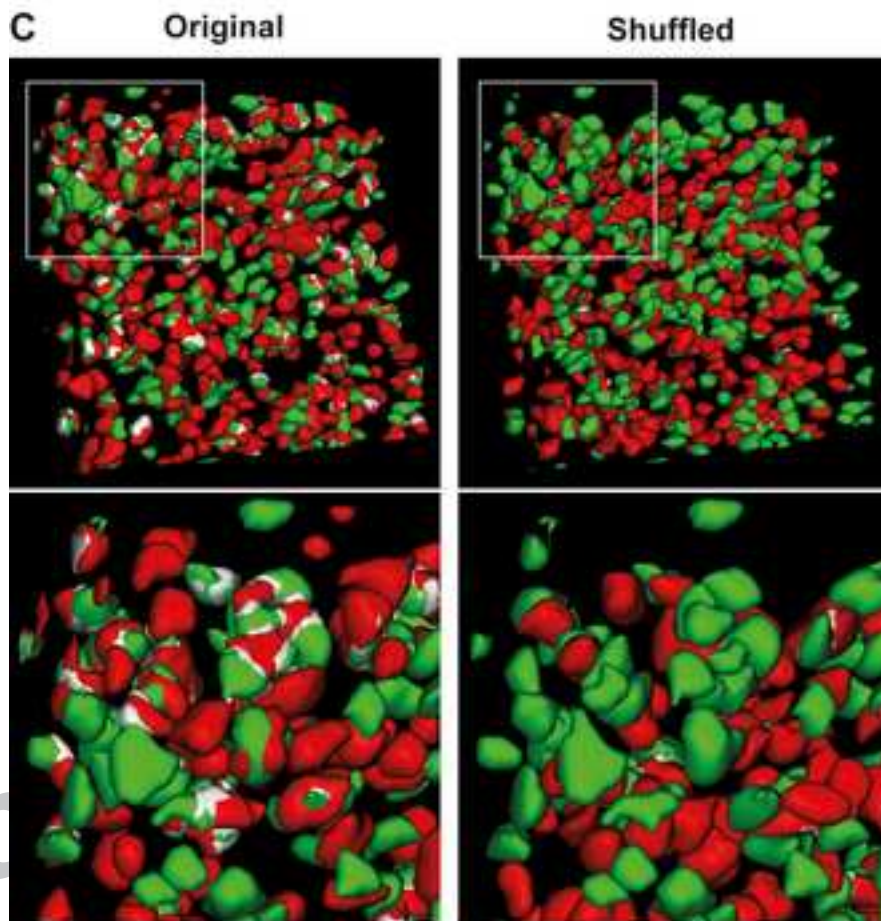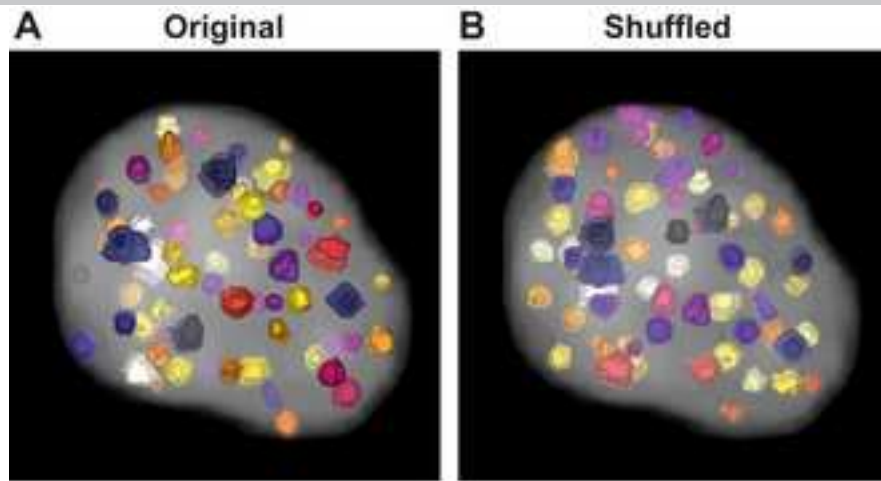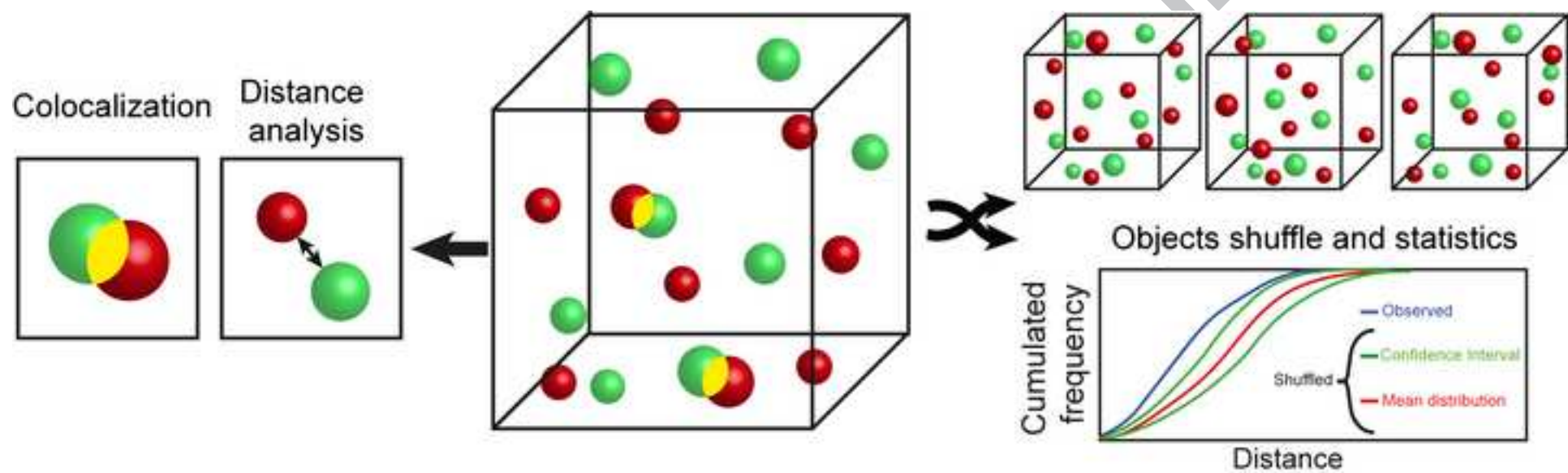
A

B

**E** Surface of contact

Figure3

**Figure4**

**Figure5**

Figure6

**DiAna, an ImageJ tool for object-based 3D co-localization and distance analysis**

Jean-François Gilles[1], Marc Dos Santos[1,2,3], Thomas Boudier[4,5], Susanne Bolte[1,*], Nicolas Heck[1,2,3,*]

**Highlights**

* A new freely available ImageJ-based plugin called DiAna is presented

* DiAna proposes two 3D procedures for image segmentation

* DiAna proposes 3D automated object-based co-localization analysis

* We introduce a novel method for statistical significance of object-based co-localization

* DiAna has extended functions for 3D distance analysis and 3D measurements